Atmos. Chem. Phys. Discuss., 13, 30097–30142, 2013
www.atmos-chem-phys-discuss.net/13/30097/2013/
doi:10.5194/acpd-13-30097-2013

Atmospheric Chemistry and Physics Discussions

On the detection of the solar signal in the tropical stratosphere

G. Chiodo[1], D. R. Marsh[2], R. Garcia-Herrera[1,3], N. Calvo[1], and J. A. García[4]

[1]Universidad Complutense de Madrid, Spain
[2]National Center for Atmospheric Research, Boulder (CO), USA
[3]Instituto de Geociencias (IGEO), Madrid, Spain
[4]Universidad de Extremadura, Badajoz, Spain

Received: 8 October 2013 – Accepted: 30 October 2013 – Published: 18 November 2013

Correspondence to: G. Chiodo (gchiodo@ucm.es)

Published by Copernicus Publications on behalf of the European Geosciences Union.

Abstract

We investigate the relative role of volcanic eruptions, El-Niño Southern-Oscillation (ENSO) and the Quasi-Biennal-Oscillation (QBO) in the quasi-decadal signal in the tropical stratosphere in temperature and ozone commonly attributed to the 11 yr solar cycle. For this purpose, we perform transient simulations with the Whole Atmosphere Community Climate Model forced from 1960 to 2004 with an 11 yr solar cycle in irradiance and different combinations of other forcings. An improved multiple regression technique is used to diagnose the 11 yr solar signal in the simulations. One set of simulations includes all observed forcings, and is thereby aimed at closely reproducing observations. Three idealized sets exclude ENSO variability, volcanic aerosol forcing, and QBO in tropical stratospheric winds, respectively. Differences in the derived solar response in the tropical stratosphere in the four sets quantify the impact of ENSO, volcanic events and the QBO in attributing quasi-decadal changes to the solar cycle in the model simulations. It is shown that most of the apparent solar-induced lower stratospheric temperature and ozone increase diagnosed in the simulations with all observed forcings is due to two major volcanic eruptions (i.e., El Chichón in 1982 and Mt. Pinatubo in 1991), that are concurrent with periods of high solar activity. While in the middle and upper tropical stratosphere, it is feasible to detect a robust solar signal, this is not the case in the tropical lower stratosphere, at least in a 45 yr record. The present results suggest that in the tropical lower stratosphere, the portion of decadal variability that can be unambigously linked to the solar cycle may be smaller than previously thought.

1 Introduction

The sun climate connection is a topic of high relevance since solar variability is one source of natural variability in the climate system. The 11 yr solar cycle is a well documented mode of variation of solar activity. To date, observations show decadal varia-

ACPD
13, 30097–30142, 2013

tions in the climate system, that are commonly attributed to the 11 yr solar cycle (see review by Gray et al., 2010). A well established decadal variability can be found in reanalysis data of stratospheric temperature (Crooks and Gray, 2005). An extended reanalysis dataset from ECMWF seems to confirm this pattern (Frame and Gray, 2010). A similar variability has also been found in stratospheric ozone in three independent satellite datasets (Soukharev and Hood, 2006).

In the tropical stratospheric domain (25° N–25° S), these studies show that zonal mean temperature and ozone vary in phase with solar activity (i.e., a warming and an ozone increase are found during peaks in solar activity). The vertical structure of the observed positive response is composed of a double peak, with maxima in the upper stratosphere at 1–3 hPa and tropical lower stratosphere (hereafter TLS) at 50–70 hPa, along with a minimum response in the middle stratosphere at 10–20 hPa (e.g., see Fig. 1 in Frame and Gray, 2010, for temperature, and Fig. 5 in Soukharev and Hood, 2006). While the upper stratospheric peak is well established and in agreement with theoretical expectations, the structure of the signal in the middle stratosphere and TLS is more uncertain, and far less understood. It has been suggested that a solar cycle modulation of tropical upwelling may be the dynamical mechanism originating the response in the TLS in ozone (Hood, 1997; Hood and Soukharev, 2003) and temperature (Kodera and Kuroda, 2002). However, this mechanism is linked to changes in wave-driving of extratropical circulation, and it is mainly operative in the winter stratosphere, where the strong variability therein makes the detection of such changes extremely challenging.

Chiodo et al. (2012) reported good agreement in the simulated vertical profile of the solar signal from the Whole Atmosphere Community Climate Model (WACCM), version 3.5, and observations. WACCM3.5 is a general circulation model with a well resolved stratosphere and interactive chemistry. Reasonable agreement was also found in other models of similar characteristics (Austin et al., 2008; Schmidt et al., 2010). However, the ability of the models in reproducing the signal in the TLS appears to depend on the boundary conditions, and the elements necessary to reproduce such a signal are

ACPD
13, 30097–30142, 2013

model dependent. For this reason, the role of additional sources of variability (e.g., ENSO, or QBO in those models which assimilate it) in the tropical lower stratospheric solar signal is far from being understood. The detection of solar signals is also difficult considering their relatively small amplitude compared with other sources of variability. This is especially true in the TLS, where a substantial portion of interannual variability is controlled by the QBO in both ozone (Randel and Wu, 2007) and temperature (Randel et al., 2009b). Another important driver for interannual variability in the TLS is ENSO (Calvo-Fernández et al., 2004; Randel et al., 2009a). Volcanic eruptions also lead to strong temperature and ozone changes in this region, where decreases of 5–10 % in ozone and a warming of more than 1 K after the Mt. Pinatubo eruption in 1991 were reported (Randel et al., 1995).

Solar signals in observations and transient simulations are usually quantified with multiple linear regression (MLR) models that include a linear trend term, and proxies for ENSO, QBO, and volcanic eruptions. Unambiguous attribution using a MLR model requires the predictors to be orthogonal (i.e., that they are not cross-correlated), and predictand time series to be serially uncorrelated. However, serial correlation in temperature and ozone exists within seasonal time scales (Tiao et al., 1990). Additionally, cross correlations between proxies may arise during certain epochs. This is the case for the QBO, which is characterized as the vertical profile of the equatorial zonal mean zonal wind. The zonal wind in the tropical stratosphere can potentially be affected by ENSO and in-situ heating caused by volcanic aerosol. Thus, volcanic and ENSO signals are embedded in the QBO index. Hence, deviations from the basic assumptions limit the reliability of estimates from regression models, especially when using data that only cover a few solar cycles, as in the case of reanalysis and satellite datasets.

The only feasible approach to quantify aliasing in observational data is to assess the sensitivity of the derived solar regression coefficients to the formulation of the regression model. This is the method used by some authors (Frame and Gray, 2010; Soukharev and Hood, 2006; Hood et al., 2010), who claimed that their solar regression

ACPD
13, 30097–30142, 2013

coefficient is clean from aliasing because of the very small changes when including ENSO, QBO, and volcanic terms in their regression model.

On the other hand, when using a climate model, the sensitivity of the simulated solar signal to the presence of other boundary conditions can be directly tested. This was done in simulations with a 2-D chemistry transport model (Smith and Matthes, 2008; Lee and Smith, 2003). Smith and Matthes (2008) showed that the simulated solar signal in tropical ozone strongly depends on the presence of the QBO. They showed that this dependence is indicative of a contamination of the solar signal by the QBO, and that the aliasing is mainly due to irregularities (i.e., departures from a sinusoidal function) in the observed QBO. In an earlier study using the same 2-D model, Lee and Smith (2003) found that volcanic eruptions have a similar effect, and that both QBO and volcanic signals equally alias on the observed structure of the ozone solar response. However, one may argue that such simplified 2-D models lacked a full description of wave-mean flow interactions that have been proposed to explain the origin of the decadal changes in the TLS.

Marsh and Garcia (2007) used a more comprehensive model to investigate tropical ozone decadal variability (WACCM3.1, Garcia et al., 2007). They found that the ozone solar signal in the TLS could only be reproduced by WACCM3.1 when observed SSTs were prescribed. They demonstrated that part of the ozone solar signal simulated in transient WACCM simulations was due to spurious correlation between the index for the solar cycle and ENSO over the 1979–2003 period. These conclusions were obtained by contrasting transient WACCM3.1 simulations performed with observed SSTs with time-slice experiments performed with climatological SSTs. Nevertheless, neither of these simulations included the radiative effects of volcanic eruptions, or a QBO. Thus, their results cannot be directly compared to observations.

There is clearly a need for a quantitative estimate of the portion of the decadal signals in the stratosphere which can unambigously be linked to the solar cycle. It has been demonstrated that a warming in the TLS, such as that commonly attributed to the solar cycle, can trigger changes in tropospheric circulation (Haigh and Blackburn, 2006).

ACPD
13, 30097–30142, 2013

Consequently, a correct attribution of changes in the TLS may in turn improve our understanding of the role of external forcings on tropospheric and surface climate that propagate downward from the stratosphere.

In this paper, we quantify the impact of the presence of other forcings on the detection of the 11 yr solar cycle signal in simulations of the WACCM3.5 version including more realistic forcing than in previous studies. WACCM3.5 is a valuable tool for this exercise, since it was previously shown that this model version is able to reproduce most features of the apparent 11 yr solar cycle observed in the tropical stratosphere over the last several decades (Chiodo et al., 2012).

We compare the amplitude of the solar signal in simulations with all observed forcings to those where a single forcing has been excluded. Differences between the simulations quantify the impact of the exclusion of each forcing on the apparent solar signal, and thus the potential aliasing from the respective sources. The solar signal is diagnosed using a novel MLR approach, which reduces the autocorrelation and improves the accuracy of the regression fit through the use of an optimal lag in the predictors.

The paper is arranged as follows. Section 2 provides a description of the model and the experimental setup, along with the statistical methods employed in the analysis. The results are outlined in Sect. 3. Section 3.1 is dedicated to the relationship between each forcing and the simulated temperature and ozone variations. Focus is then given on the 11 yr solar cycle signal in Sect. 3.2. The robustness of the apparent solar signal in the reference case is assessed in Sect. 3.3. A generic discussion of the results and their implications is given in Sect. 4, while Sect. 5 summarizes the main results and conclusions.

ACPD
13, 30097–30142, 2013

2 Data and methodology

2.1 Model simulations

WACCM3.5 is an improved version of the WACCM3.1 general circulation model (Garcia et al., 2007). The standard resolution of 66 vertical levels ranging up from the surface to the thermosphere (140 km), and 1.9° latitude by 2.5° longitude in the horizontal was used in this work. This is the same model version that participated in the CCMVal-2 activity (CCMVal-2, 2010). Details of the model relevant for simulating the 11 yr solar cycle are discussed in Chiodo et al. (2012).

We performed pairs of simulations of WACCM3.5 model run from 1960 to 2004. The set-up of one pair is identical to the REFB1 type of simulations presented in Eyring et al. (2010) for a comparison with other Chemistry Climate Models and in Chiodo et al. (2012) for a detailed analysis of the 11 yr solar cycle signal. It is named here as "all forcings" due to the inclusion of all known natural and anthropogenic forcings. The forcings include observed SSTs and sea-ice concentrations (Hurrell et al., 2008), loadings of GHG and ozone depleting substances. Model equatorial stratospheric winds are relaxed toward observed winds to obtain a realistic time-varying QBO (Matthes et al., 2010). The effects of volcanic eruptions are included by prescribing aerosol surface area densities (SAD) from the SAGE II measurements (Thomason et al., 1997), and the impact on the heating rates in the stratosphere is explicitly calculated (Tilmes et al., 2009). The 11 yr solar cycle in solar irradiance is introduced in the model by prescribing spectral irradiance data modeled by Lean et al. (2005), integrated over specific model bands for radiation and chemistry calculations. This set of simulations is aimed at closely reproducing observed interannual variations in the tropical stratosphere, and serves as a reference case.

In the second set of experiments, named "fixedSSTs", a climatological seasonal cycle of the SSTs is prescribed, thus removing ENSO from possible sources of variability in the stratosphere. In the next set called "noQBO", the tropical stratospheric winds are not relaxed towards observations. Since the model version used in this work does

ACPD
13, 30097–30142, 2013

not spontaneously generate a QBO, permanent weak easterlies in the tropical stratosphere are simulated. Finally, the fourth set named "noVOLC" is forced with a constant seasonal cycle of SAD, thus excluding peaks in sulfate aerosol concentrations in the stratosphere due to volcanic eruptions. The list of experiments is given in Table 1.

2.2 Analysis method

Monthly mean output is averaged over the two realizations done for each of the four sets, season (DJF, MAM, JJA, SON), longitude, and the 25° N–25° S latitude band. The tropical average seasonal mean anomalies are used as input for an improved MLR technique, whose formulation is novel in the context of solar cycle studies. Details are described in the Appendix and are briefly outlined below.

First, the autocorrelation is removed following a Box-Jenkins pre-whitening procedure (Box and Jenkins, 1980). This is applied on the time-series of the seasonal means of the simulated ozone and temperature and of the predictors (i.e., the forcings used in each set). Next, lags are calculated that maximize the absolute value of the correlation between the prewhitened field variable and the forcings. In this way, the projection of the field variable onto the forcings in each set is maximized. These steps have been extensively used in the formulation of multiple linear regression models in other fields (e.g. in biometeorology, Diaz et al., 2002a, b and economic forecasting, Bisgaard and Kulahci, 2011), though they are new in the analysis of the 11 yr solar signal.

The suitable lag for each predictor must be chosen with care. Ideally, the lag correlations should represent a physically consistent relationship between the predictand and predictors. On the other hand, such lags should not bring different predictors into phase, thereby increasing collinearity. With these criteria in mind, an optimal window, over which the suitable lag is searched for, is identified.

In our analysis, we use zonal wind time-series at 30 and 10 hPa, which serve as QBO indices in the regression. By using the residual of a regression of the zonal wind onto other indices (details are described in the Appendix), the QBO indices become orthogonal to the other predictors. Additionally, we keep the mutual phase relationship

ACPD
13, 30097–30142, 2013

by using the same time lag in both indices. We find that by using this technique, the cross correlation among the QBO indices and the other predictors never exceeds 0.06, which ensures that the null-hypothesis of no correlation cannot be rejected at the 99 % confidence level.

Principal component analysis (PCA) has been used in previous studies to derive orthogonal QBO indices (Randel and Wu, 1996; Crooks and Gray, 2005; Frame and Gray, 2010). The mathematical orthogonality constraint can potentially limit the physical realism of the principal component associated with the QBO. For this reason, we believe that the residuals from a MLR at 30 and 10 hPa are more directly linked to the original wind field at both heights, and thus more suited than principal components for representing the QBO variability in the MLR.

This procedure is repeated for each of the simulation sets, to both temperature and ozone. The regression model formulated in Eq. (A6) is applied at constant pressure levels of the tropical stratospheric domain (0.1–100 hPa).

The MLR includes only predictors for those forcings included in the specific set of experiments (e.g. no QBO term is used in the analysis of the "noQBO" set). Since the main focus of this paper is the detection of the solar signal in the tropical stratosphere, results from the regression analysis are only presented for the UV coefficient (β'_{uv} in Eq. A6). The coefficient has been scaled at all isobaric levels by 0.175. This scaling factor is the 2σ value of the UV radiation index used in the MLR, which represents the peak to trough solar cycle variation in units $\mathrm{W\,m^{-2}\,nm^{-1}}$.

3 Results

Figure 1 shows the time-series of the tropical average (25° N–25° S) seasonal mean anomalies of the zonal mean temperature at the 50 hPa level from the "all forcings" set. A long-term cooling trend is evident, and the amplitude of approximately $-0.5\,\mathrm{K\,decade^{-1}}$ agrees with observations (Randel et al., 2009b). The trend is inter-

ACPD
13, 30097–30142, 2013

rupted by positive peaks over 2 K in 1964 and 1992, which are caused by two major volcanic eruptions (Mt. Agung and Mt. Pinatubo).

Before applying the MLR, the variables and the forcings are prewhitened with the autocorrelation coefficient of the field variables. Since the choice of the lag for the predictors is crucial to improve the regression fit, we first analyze the lag correlation between forcings and the simulated field variables temperature and ozone.

3.1 Lag correlation analysis

The optimal lag must ensure a physically consistent relationship between the prewhitened field variables and the forcings. For this purpose, the vertical structure of the lag correlation is analysed in detail, in order to identify a window representing a realistic time-scale for the response in the selected variable to each of the applied forcings.

Figure 2 shows the vertical profile of the correlation of the tropical average seasonal mean temperature with UV radiation from the "all forcings" set, plotted as a function of the time lag in a window of 10 yr (−5 to +5), thus covering an almost complete solar cycle. Correlations at positive lag values mean that variations in the predictors lead the simulated variable, while the opposite is true for negative lags. In Fig. 2, positive lags imply that UV changes lead temperature changes.

Although the pre-whitening of the time-series considerably reduces the magnitude of the correlations, a well defined structure propagating downward is evident. A positive temperature-UV relation is found at 1 hPa, which lingers for 2 yr around the peak of solar activity, and negative values can be seen 5 yr prior and after the peak in UV radiation, indicating a cooling around minima of solar activity. The positive correlations in the middle and lower stratospheric levels (10–50 hPa) show maxima with a lag of around 1, 2 and 3.5 yr. In the lowermost stratosphere (50–100 hPa), values exceeding 0.15 are found at lags of 1 to 3 yr. This suggests that the warming induced by peaks in solar activity is instantaneous in the upper stratosphere, whereas it is weaker in amplitude and delayed by approximately 1 yr in the lower layers. Overall, the lag correlation to the UV

ACPD
13, 30097–30142, 2013

in the WACCM simulations depicts a downward propagation of the solar signal. This is consistent with the "top-down" mechanism involving a downward pathway (which is thus mediated by the stratosphere) for solar influences to impact surface climate, as hypothesized in previous studies (Meehl et al., 2009; Gray et al., 2010).

A downward propagating pattern is also found in the lag correlations between temperature and zonal wind at 30 hPa (not shown). It is associated with the secondary circulation triggered by the imposed QBO (Baldwin et al., 2001), which is externally imposed by nudging the model to observed wind values. The correlations with N3.4 and SAD indices suggest that the response to these forcings is rather instantaneous and mostly localized in the TLS (not shown). Negative correlations with the N3.4 index are found to be significant in the TLS between lags of 0 and 1 yr, maximising at 3–5 months lag (or 1 season), which is consistent with the lagged impact of ENSO on the TLS reported elsewhere (Marsh and Garcia, 2007; Calvo et al., 2010). In the TLS, a strong peak of positive correlation with the volcanic SAD index is found at zero lag, which decreases rapidly as the lag is increased to around 18 months. This agrees with the estimates of the time-scale of the stratospheric warming observed after volcanic eruptions (Robock, 2000). At lags larger than 1 yr, some downward propagating QBO-like correlation structures are found in both the N3.4 and SAD indices. Such correlations do not have a physical meaning, since they are related to spurious interference with the QBO. Hence, lags larger than 1 yr have not been used in the MLR for temperature.

Similar to temperature, the lag correlation of UV radiation with tropical mean ozone is shown in Fig. 3 for the "all forcings" set. As it occured in zonal mean temperature, a broad structure of positive correlations with the UV radiation appears around lag 0 in the upper stratosphere. Positive values are also found at lag 0 in the TLS. The positive ozone-UV relation in the middle and upper stratosphere is due to the UV-induced photolysis of molecular oxygen, and recombination with atomic oxygen (Pap and Fox, 2003). Unlike in temperature, there is less evidence of a lagged response in the TLS. The larger lag in temperature compared to ozone may indicate that different processes are controling the apparent solar cycle response in both variables.

ACPD
13, 30097–30142, 2013

In the TLS, a strong negative correlation of ozone with the N3.4 index is evident at lags up to 1 yr, maximizing at around 7 months (not shown). At zero lag, a positive correlation is evident at 1–10 hPa. Both the ozone-ENSO out-of-phase variation in the TLS, and the in-phase variation in the middle stratosphere are consistent with previous studies (Hood et al., 2010). At zero lag, a similar structure of negative correlations in the TLS, with positive correlations aloft, is also found between ozone and the volcanic SAD index (not shown). The negative ozone-SAD correlations in the TLS indicate that tropical mean ozone is depleted by chemical processes initiated by the volcanic aerosol in the stratosphere. This qualitatively agrees with the ozone changes observed after the Mt. Pinatubo eruption (Robock, 2000).

We find that a suitable window for the choice of the optimal lag is comprised from 0 to 1 yr for both temperature and ozone, as this minimized the cross correlation between predictors (not shown). Thus, the optimal lag maximizing the correlation with the UV index (i.e., $\tau_{i=\mathrm{uv}}$ in Eq. A6) is identified in this window.

The vertical profile of the optimal lag is shown in Fig. 4 for zonal mean temperature and ozone. We show the values obtained for the "all forcings" case (a), and for the three idealized sets (b–d). Overall, the temperature-UV and the ozone-UV correlation patterns are found to be qualitatively similar in the three simulation sets excluding single forcings (not shown), which explains the similarity in the vertical profile of the optimal lag. In the case of zonal mean temperature, the profile shows a downward progression in all four cases, with a lag of 1 yr in the TLS, consistent with the lagged positive correlation in this region seen in Fig. 2. In tropical ozone, the lag needed to maximize the correlation in the TLS is smaller than in temperature. For both temperature and ozone, no lag is taken for the SAD index, since the strongest correlation is found at lag 0 (not shown). A lag of 0.5 yr (or 2 seasons) is taken in the TLS for the N3.4 index, in agreement with previous studies (Marsh and Garcia, 2007). With these values for τ, a regression of the time-series of zonal mean wind at 10 and 30 hPa is performed. The residuals are then taken as QBO indices (i.e., $u10^*$ and $u30^*$ in Eq. A6).

ACPD
13, 30097–30142, 2013

An example of the application of the MLR procedure employed in this paper is given for the tropical average zonal mean temperature at 50 hPa, which is the time-series shown in Fig. 1. Figure 5a shows the temperature time-series after pre-whitening, along with the fit output from the MLR model formulated in Eq. (A6). The optimal lag used is 0.75 yr (or 3 seasons) for the UV index (as seen on Fig. 4), 0.5 yr (or 2 seasons) for N3.4, while no lag is used for SAD and both QBO indices. It is found that while the pre-whitening smooths part of the variability, the peaks of the original time-series shown in Fig. 1 are preserved. The r^2 value of 0.4 implies that 40 % of the variability in the prewhitened temperature time-series can be explained by the regression fit. Note that if no optimal lag is used for the predictors, the r^2 value would be 0.2, which indicates a less accurate fit (not shown). Figures 5b–f plot the contribution of each term on the right hand side of Eq. (A6) to the regression fit shown in Fig. 5a. The strongest temperature changes are caused by volcanic eruptions, with Mt. Pinatubo generating a 3 K anomaly (Fig. 5f). Changes of 0.5–1 K are associated with the $u30^*$ index (i.e., the zonal wind at 30 hPa) and ENSO (Fig. 5c–d). On the other hand, the 11 yr solar cycle signal is smaller, with temperature deviations of a few tenths of a K (Fig. 5b).

3.2 The 11 yr solar cycle signal

The vertical profile of the solar signal, shown as the UV regression coefficient of the tropical average (25° N–25° S) zonal mean temperature scaled by 2σ of UV radiation, is shown in Fig. 6. The profile is shown for the reference "all forcings" set, and the idealized experiments, using the optimal lag for the UV index shown in Fig. 4.

In the "all forcings" set (black line in Fig. 6), a statistically significant UV-induced warming is found throughout the tropical stratosphere, with maximum values of 0.8 K at 1 hPa and a secondary maximum of 0.6–0.7 K at 40–50 hPa. It is interesting to note that a statistically significant solar signal is also extracted in the middle stratosphere at 10 and 20 hPa, even though this is a region of relative minimum response. The lag used for the UV index is 0 at 1 hPa, 6 months at 10 hPa, and 9 months between 30 and 70 hPa (see Fig. 4). Thus, the warming in the upper layers is an instantaneous

ACPD
13, 30097–30142, 2013

response, whereas the maximum in the lower layers is lagged. If the UV index is not lagged, the apparent solar response at 50 hPa is reduced by 40 % (not shown).

In the "fixedSSTs" case (red line in Fig. 6), the simulated temperature solar signal is similar to the reference case, although the secondary maximum at 50 hPa is obtained at a slightly larger lag compared to the other sets (t = 1 yr, see Fig. 4). The strong similarity in the derived UV regression coefficient in temperature suggests that the ENSO contribution to the apparent solar signal is negligible. The low sensitivity of the UV regression coefficient to the inclusion of ENSO is not due to the removal of the serial correlation, as similar results are obtained without pre-whitening the data (not shown). The "noQBO" set (green line in Fig. 6) shows a significant solar response throughout the stratosphere above 60 hPa, with a peak of 0.8 K at 50 hPa. Overall, the profile obtained resembles the reference "all forcings" case, although a slighly stronger magnitude of the warming is evident in the TLS. In the "noVOLC" set (blue line), a significant regression coefficient is obtained at all levels above 20 hPa, with a peak of 0.7 K at 1 hPa. However, below 20 hPa the signal becomes weak and not statistically significant. Thus, no robust temperature response is obtained in the TLS in the WACCM simulations that do not include volcanic eruptions. The absence of a response indicates that the apparent lagged temperature solar signal in the TLS diagnosed in all other simulation sets is associated with the effect of volcanic aerosols.

A similar reduction in the apparent signal in the "noVOLC" set is seen when using a standard MLR without BJ pre-whitening and without lagging the UV index (not shown). Using a standard MLR, a different response is also obtained in the "fixedSSTs" and "noQBO" cases (not shown). Compared to the "all forcings" case, the UV regression coefficient for temperature in the TLS is higher in the "fixedSSTs" set, while it is weaker in the "noQBO" case. This suggests that the MLR method formulated here allows for better separation of the temperature solar signal from ENSO and QBO.

The MLR was also applied to the tropical average zonal mean ozone mixing ratio simulated by WACCM. The vertical profile scaled by 2σ of the UV radiation is shown in Fig. 7 in terms of relative solar cycle (%) peak to trough change in the mixing ratio

ACPD
13, 30097–30142, 2013

using the lag values for the UV index shown in Fig. 4. In the "all forcings" case, there is a well defined double peak structure, with statistically significant ozone increase in the middle and upper stratosphere peaking at 2 % near 10 hPa, a relative minimum at 30 hPa, and a significant increase at 40 hPa and below, peaking at 3.5 % between 70 and 90 hPa.

Fairly good agreement among the experiments is seen in the UV-induced ozone increase of 1.5 % at 5–10 hPa. At 20 hPa, the solar cycle ozone response in the "noVOLC" and "noQBO" case is slightly stronger than in the "all forcings" case. Reasonable agreement is evident in the relative minimum (and non-significant) response at 30 hPa, with exception of the "noQBO" case, which shows a positive and significant ozone response of 1 %. The difference between the regression coefficients from the "all forcings" case and "noQBO" at 30 hPa is statistically significant, thus indicating that QBO interferes with the solar cycle analysis thereby reducing the apparent solar signal at this height, giving rise to the relative ozone minimum response.

Significant differences are evident in the amplitude of the ozone increase in the stratospheric levels between 40 and 100 hPa. While the "all experiment" case features a significant ozone increase ranging from 1.5 % at 50 hPa to 3.5 % at 70 hPa, the response in the "noVOLC" case follows a similar profile, although with lower values ranging from a non-significant 0.6 % increase at 50 hPa, to 1.5–2 % at 70–80 hPa. At 70 hPa and below, a different response is also observed in the "noQBO" case, where a non-significant 1–1.5 % ozone increase is obtained. On the other hand, the ozone response at 70–80 hPa is increased to 3.8 % in the "fixedSSTs" case, although the difference in the response between this and the "all forcings" case is not significant. A similar behavior is observed between 80 and 100 hPa. Among all experiments, the ozone profile obtained from the "fixedSSTs" set is the one that most closely resembles the "all forcings" case. Those calculated from the "noVOLC" and "noQBO" exhibit the largest differences, with a weaker response throughout the lower stratosphere below 50 hPa in the "noVOLC" case, and below 70 hPa in the "noQBO" case. This suggests that part of the apparent lower stratospheric ozone signal obtained from the "all forc-

ACPD
13, 30097–30142, 2013

ings" case is due to QBO and volcanic aliasing, with the largest spurious contribution coming from volcanic aerosol.

Note that if a standard MLR is used (without pre-whitening and lagging the UV index), an increase of 6 % is obtained in lower stratospheric ozone in the "fixedSSTs" set, which is significantly stronger than in all other cases (not shown). This indicates that the use of the MLR technique formulated in this work reduces ENSO aliasing in ozone. It is also found that even stronger differences in the ozone UV regression coefficient would be obtained between the "noQBO" and "all forcings" cases if raw wind time-series are used as QBO indices in the MLR (not shown). Thus, the use of filtered QBO indices allows for better separation of QBO and solar signals in the TLS.

3.3 Sensitivity of the solar signal to the data window

The results from the idealized cases give useful information about the impact of other forcings on the analysis. However, they do not apply to the real atmosphere since it is plausible that such simulations were not able to reproduce a non-linear interaction between the missing forcing and the 11 yr solar cycle. The aim of this section is to assess aliasing in the regression of one single record, which is driven by the combination of forcings that most closely resembles the real atmosphere, as is the "all forcings" case. In this way, it is possible to quantify the potential aliasing in regressing a limited record, and in turn to infer the feasibility of extracting a robust solar signal from the window covered by observational records. One method to accomplish this consists of testing the sensitivity of the diagnosed signal to the length of the data.

We calculate the UV regression coefficient from the "all forcings" set for a varying data window, whose endpoint is the last year available in the simulations: 2004. A minimum of 10 yr is used to cover the last solar cycle (1995–2004), and the data window is gradually extended to the whole 45 available years, using 1 yr increments.

Figure 8 shows the estimates for tropical mean temperature, calculated at 5 different pressure levels representative of the upper stratosphere (1 hPa), middle stratosphere (10 hPa), and lower stratosphere (30, 50, and 70 hPa). Note that the end-point value

ACPD
13, 30097–30142, 2013

obtained with the entire 45 yr time series is identical to that shown (on the same levels) in Fig. 6.

In the upper stratosphere at 1 hPa (Fig. 8a), a constant value of 0.8–1.0 ± 0.2 K is obtained. One can deduce that the minimum number of years necessary for extracting a significant and stable solar signal in temperature at 1 hPa is 10–15 yr, since the value obtained with such window is fairly close to that calculated with the full available period of 45 yr. At 10 and 30 hPa (Fig. 8b–c), the regression coefficient is slightly negative and not significant when less than 20 yr of data are used. It then stabilizes to a significant positive value of 0.4 ± 0.2 K at 10 hPa and 0.5 ± 0.3 K at 30 hPa when more than 25 yr of data are used.

At lower stratospheric levels (50 and 70 hPa, shown in Fig. 8d–e), the derived values are more uncertain than in the upper stratosphere, as indicated by the wider error bars, and exhibit stronger sensitivity to the window length. Broadening the data window reduces the apparent signal at 50 and 70 hPa from 1.0 ± 0.7 K with 15 yr of data to 0.2–0.5 ± 0.3 K when using the 45 yr of data. No convergence towards a steady value is found at these levels. Thus, a stable and significant temperature response can only be detected above 30 hPa, while a different behavior is observed at 50 and 70 hPa, where no robust value can be extracted with the available 45 yr long record.

For three stratospheric levels (i.e., 30, 50 and 70 hPa), the UV regression coefficient is also estimated with the same regression procedure using MERRA reanalysis data (Rienecker et al., 2011), chosen here over other reanalysis products due to the larger overlap with the simulations (1979–2004). WACCM and MERRA can be directly compared by using 26 yr as the window in the "all forcings" case. At this window length, the apparent solar signals at 30 hPa (Fig. 8c) 50 hPa (Fig. 8d) and 70 hPa (Fig. 8e) of respectively 0.3, 0.5 and 0.7 ± 0.2 K in the simulation agree well with the values obtained from MERRA, thus indicating that the model is able to reproduce the observed apparent solar cycle response at these levels.

In addition, strong swings are evident in the middle and lower stratosphere (30, 50 and 70 hPa) a few years after the occurrence of the two major volcanic eruptions when

ACPD
13, 30097–30142, 2013

using WACCM data, suggesting that volcanic and solar signals cannot be cleanly separated by the regression model at these levels. Interestingly, both Mt. Pinatubo and El Chichón eruptions appear to interfere with the solar signal at 30 and 50 hPa. This is not the case at 70 hPa, where only the former has a discernible impact (Fig. 8e). Overall, the peak associated with the volcanic eruptions disappears after 30 yr of data are included in the regression analysis. Even when the analysis is extended using a longer window, the UV coefficient decreases at both levels, which is particularly evident at 70 hPa. This suggests that in WACCM3.5, no robust signal in temperature can be extracted in the TLS with 45 yr of simulations data.

Figure 9 shows the UV regression coefficient obtained at 50 and 70 hPa when periods after El Chichón and Mt. Pinatubo eruptions are omitted (June 1982–November 1983 and September 1991–November 1993). During such periods, the peaks in lower stratospheric temperature associated with the SAD index can be identified (see Fig. 5f). Convergence toward a constant value of approximately 0.1 ± 0.2 K is obtained when more than 20 yr of data are used. However, this value is not significantly different from zero. When the same years are excluded from the MERRA reanalysis data, the UV coefficient is also reduced from $0.6–0.7 \pm 0.3$ K to 0.2 ± 0.4 K at both 50 and 70 hPa. This indicates that when applying MLR methods on stratospheric temperature data covering 25 yr, a better separation of solar and volcanic signals can only be achieved with removal of data around both El Chichón and Mt. Pinatubo eruptions. This is consistent with the absence of a signal in the TLS in the set without volcanoes (blue line on Fig. 6).

Similar results for zonal mean ozone are shown in Fig. 10. The ozone solar signal is robust to the extension of the data window at 1 hPa (Fig. 10a), and a constant and significant ozone increase of 0.7 ± 0.4 % is found after 10 yr of simulations data. At 10 hPa (Fig. 10b), positive and significant values of 2 ± 0.8 % are found for all data windows, although jumps to higher values are evident when using less than 30 yr of data. A significant positive UV coefficient is obtained at 30 hPa when using less than 15 yr of data (Fig. 10c). However, this signal is not real since no significant ozone-UV relationship

ACPD
13, 30097–30142, 2013

is obtained with a larger data window. This is the region in which a relative minimum response in the vertical profile is obtained in all idealized experiments, although with slightly different magnitudes (see Fig. 7). At 30 hPa, the "noQBO" experiment showed a significant ozone increase of 0.6 % (see Fig. 7), which suggests that QBO aliasing reduces the apparent 11 yr variation at this level.

At 50 and 70 hPa, a strong swing in the ozone UV response from negative to positive values is evident in proximity of the Mt. Pinatubo eruption in 1991 (Fig. 10d–e), which is indicative of the volcanic aliasing when regressing data of Mt. Pinatubo eruption. There is little evidence of aliasing in the wake of the El Chichón eruption in 1982 at 50 hPa. At this level, a rather constant and marginally significant value of 1.0–1.5 ± 1.0 % is diagnosed when more than 20 yr of data are used.

At 70 hPa (Fig. 10e), there is also a jump in proximity of the El Chichón eruption in 1982, although the magnitude is smaller than in the years around Mt. Pinatubo (1991). Overall, volcanic eruptions have a stronger impact on the signal at 70 hPa than at 50 hPa, which is consistent with the larger differences found at this level in the "noVOLC" set. The error bars and the variations in the amplitude are larger than at higher levels, which suggests that it is not feasible with the available data to extract an accurate estimate for the ozone solar response at 70 hPa. Nevertheless, there is some evidence of a trend toward a positive signal of 3.0 ± 1.5 % as all available 45 yr of data are included in the analysis.

Figure 11 shows the ozone UV coefficient calculated at 50 hPa and 70 hPa, when the El Chichón and Mt. Pinatubo post eruption data are omitted following the same procedure taken for temperature. A fairly constant value of 2.0 ± 1.5 % is obtained at 50 hPa when using more than 25 yr of data. These numbers are not significantly different from those shown in Fig. 10d, which were calculated with Mt. Pinatubo and El Chichón data retained. At 70 hPa, there is nearly no response at a window of 20–25 yr, and a positive trend towards positive values is evident when more than 35 yr of data are used. The value of 2.0 ± 1.6 % obtained with the full 42 yr window is lower than the 3.0 ± 1.5 %, which was diagnosed without removing post eruption data (Fig. 10e). This is consistent

ACPD
13, 30097–30142, 2013

with the reduction in the apparent solar signal obtained from the "noVOLC" experiment (Fig. 10).

Overall, temperature and ozone show different sensitivities to data windowing, which probably owes to the different processes controlling their variations in the tropical stratosphere. Further complication is brought by the low signal to noise ratio in ozone due to the relatively small ozone concentrations below 50 hPa. Nevertheless, both variables suggest that a robust solar signal can only be extracted using an MLR technique at upper and middle stratospheric levels.

4 Discussion

The tropical mean vertical profile of the 11 yr solar signal has been extracted from WACCM simulations using a novel MLR methodology. In the upper stratosphere, the 0.8 ± 0.2 K warming agrees with ERA-40/ERA-Interim estimates within the levels of uncertainty (see Fig. 1 in Frame and Gray, 2010). A robust and statistically significant signal is extracted at 1 hPa using a 15–20 yr window, which is covered by stratospheric observational records. At 10 hPa WACCM shows a significant warming of 0.3 ± 0.1 K obtained, whereas ERA-40 and ERA-Interim data show no significant response. We found that this difference is due to the new MLR method used in this study. Between 30 and 70 hPa a significant warming of $0.5–0.7 \pm 0.3$ K is diagnosed in WACCM, which agrees with values reported from ERA-40/ERA-Interim reanalysis in Frame and Gray (2010). Similar numbers are also calculated from MERRA reanalysis at 30, 50 and 70 hPa over the same period (1979–2004, see Fig. 8e). It is found that more than half of the temperature increase in this region is due to the use of a 1 yr lag in the UV index. Without using a lagged UV index, a warming of 0.3 to 0.4 ± 0.2 K would be obtained, which is in better agreement with the values obtained using a standard MLR on WACCM3.5 simulations driven with the same forcings (Chiodo et al., 2012) (see their Fig. 2a).

ACPD
13, 30097–30142, 2013

It is clear from Fig. 6 that the warming at 30 hPa and lower levels disappears in the set without volcanic forcing, which suggests that aliasing of the volcanic aerosol signal increases the apparent solar signal. Further evidence of this comes from the increase in the UV regression coefficient when the boundaries of the data window considered for regression analysis overlap the years of the Mt. Pinatubo and El Chichón eruptions (Fig. 8c–e). There is also a tendency towards smaller values of the UV regression coefficient in the lower stratosphere (50–70 hPa) as more years are added to the analysis, although no convergence towards a stable value is obtained even with a 45 yr window. This suggests that it is not feasible to extract a robust signal in this region over the recent past. The spurious contribution of volcanic aerosols to the UV regression coefficient is especially pronounced when using records covering 2 to 3 decades, as in MERRA reanalysis data. Better separation of solar and volcanic signals in temperature can be achieved by excluding El Chichón and Mt. Pinatubo post eruption data from the analysis, since convergence toward a stable (and non-significant) signal is obtained in this way (shown in Fig. 9). Additionally, extending the observational data record to cover solar cycles without volcanic eruptions coincident with peaks of solar activity (as e.g., solar cycle 23) decreases the apparent solar-induced warming in the middle and lower tropical stratosphere. This is seen when regressing onto a 31 yr long ERA-Interim/ERA-40 merged dataset of 1978–2008 instead of the 23 yr ERA-40 data of 1979–2001 (Frame and Gray, 2010) (see their Fig. 1).

The ozone increase of 2 ± 0.7 % in the upper stratosphere at solar maximum in the "all forcings" WACCM simulation agrees well with SBUV and SAGE observations (Soukharev and Hood, 2006; Randel and Wu, 2007). The response at these levels is robust, since it is stable over time, and it is also diagnosed in the idealized experiments. An accurate estimate can be extracted with 20–25 yr of data, which is a window covered by satellite data. A relative minimum response in tropical ozone is diagnosed in WACCM around 30 hPa. This structure resembles the non-significant negative response seen at 10 hPa in SBUV and SAGE (Soukharev and Hood, 2006; Randel and Wu, 2007). As in temperature, we find that there is a mismatch in the height of the

ACPD
13, 30097–30142, 2013

relative minimum response from the model and reanalysis that is due to the different MLR methods used (not shown).

A significant ozone increase is found in the lower stratosphere between 40 and 100 hPa, with values ranging from 2 ± 1.2 % at 50 hPa to 3.5 ± 2.0 % at 80 hPa. Similar numbers have been previously reported for the same period covered by SAGE and SBUV data (see Fig. 12a in Randel and Wu, 2007, and Fig. 8 in Soukharev and Hood, 2006), although no comparison with these studies is possible below 50 hPa, as this is the lowest boundary in the available satellite data of stratospheric ozone. Idealized experiments show that ENSO aliasing in the lower stratospheric ozone signal is negligible. This is due to the combined use of lagged ENSO and UV terms in our regression model and to a sufficiently large window of 45 yr, which is in line with the findings of Marsh and Garcia (2007). On the other hand, it is also found that the apparent solar cycle ozone increase in the lower stratosphere is strongly influenced by volcanic aerosols and, to a lesser extent, by the presence of the QBO. Interference with volcanic eruptions is also indicated by the increase in the UV regression coefficient when the data window overlaps periods shortly after Mt. Pinatubo and El Chichón eruptions (Fig. 11c–e). Our results confirm the findings from a study using a more simplified 2-D transport chemistry model that pointed to a strong contribution of the QBO and volcanic aliasing on the tropical ozone solar signal (Lee and Smith, 2003; Smith and Matthes, 2008).

We note that between 20–30 hPa a consistent bias is seen in both temperature and ozone related to the problem of volcanic heating aliasing, even though the MLR fits are carried independently for temperature and ozone. Specifically, it appears a fraction of the volcanic-induced heating is mis-attributed to the solar cycle by the MLR, thus producing warmer temperatures during solar maximum. This diabatic heating produces stronger upwelling rates in the simulations including all observed forcings compared to the set excluding volcanic forcing. Due to the strongly positive vertical gradient in ozone mixing ratio, the increased upwelling results in an apparent ozone decrease, which the MLR also attributes to the solar cycle (leading to a weaker solar-cycle ozone response relative to the set excluding volcanic aerosols). On the other hand, the positive bias

ACPD
13, 30097–30142, 2013

in both temperature and ozone solar signals below 50 hPa remains to be explained in dynamical terms. At these levels, it may be difficult to find a plausible mechanism because of the relatively small ozone concentrations, and thus low signal-to-noise ratio.

Chiodo et al. (2012) showed that the temperature and ozone signal in the TLS estimated is stronger and closer to observations in the WACCM3.5 model than in the WACCM3.1 version. The improvement is likely a consequence of WACCM3.1 not assimilating a QBO and the omission of volcanic aerosol heating in the simulations (Garcia et al., 2007). Consequently, the QBO and volcanic signals did not map into the 11 yr solar cycle in the regression analysis of transient WACCM3.1 simulations, leading to a worse agreement compared to transient WACCM3.5 simulations. However, the better agreement with observations does not necessarily imply a better estimate of the solar signal. In conclusion, the present results suggest that either given a long enough window, or in idealized experiments excluding the spurious contribution of volcanic aerosols in the analysis, a consistent, though weaker than previously thought, solar response is diagnosed in the tropical lower stratosphere.

5 Summary

We have investigated the attribution of quasi-decadal variations in tropical stratospheric temperature and ozone to the 11 yr solar cycle. To do so, we perform a set of transient WACCM3.5 simulations with different combination of forcings. The solar signal is extracted from the model simulations using a new MLR approach, which (i) reduces the autocorrelation through pre-whitening and (ii) improves the accuracy of the fit through the use of an optimal lag. The design of the model experiments employed here is more realistic than previous modeling studies on the impact of aliasing on the detection of the solar signal, as e.g. Marsh and Garcia (2007). The main findings are as follows.

– A double-peak profile in both temperature and ozone with maxima in the upper and lower stratosphere is diagnosed in the WACCM3.5 simulations forced with all observed forcings. This agrees qualitatively well with reanalysis and satellite data.

ACPD
13, 30097–30142, 2013

– In the tropical lower stratosphere, a substantial portion of the apparent solar-induced increase in temperature and ozone is related to volcanic aerosol. This is due to alignment of two major volcanic eruptions (El Chichón and Mt. Pinatubo) with peaks of solar activity during cycles 21 and 22.

– Using 45 yr of data, a robust 11 yr solar signal can only be extracted above 10 hPa. At lower levels, longer records would be required. This occurs because the solar and volcanic signals cannot be adequately separated.

– The aliasing issue is ameliorated if windows around El Chichón and Mt. Pinatubo are excluded from the analysis (June 1982 to November 1983, and September 1991 to November 1993). This removal would greatly reduce the apparent solar signal in temperature. In ozone, further complication is caused by interference with the QBO.

It is plausible that the observed amplitude of the solar-induced increase in the TLS in temperature and ozone (as reported in other studies, 0.8 K in reanalysis (Frame and Gray, 2010) and 4 % in satellite data (Soukharev and Hood, 2006)) is overestimated due to issues associated with the MLR analysis of a too short record that have been explored in this work.

The present results suggest that MLR techniques require the use of longer observational records for unambigous separation of decadal changes driven by the solar cycle. When regressing reanalysis and satellite data, which are available to date (as e.g., MERRA reanalysis data spanning over 26 yr), both windows around El Chichón and Mt. Pinatubo should be removed for more accurate determination of the solar signal.

ACPD
13, 30097–30142, 2013

Appendix A

The standard version of multiple linear regression models takes the following form:

$$Y_t = \sum_{i=1}^{n} \mathbf{X}_{i,t}\beta_i + \epsilon_t \quad \text{(A1)}$$

where Y is the predictand (i.e., the dependent variable); t is the time dimension; $\mathbf{X}$ is a matrix with the basis functions containing n predictors, β are the regression coefficients, and ϵ is the residual error term.

Multiple linear regression models after Eq. (A1) are commonly used in solar cycle studies. The $\mathbf{X}$ matrix typically contains a set of predictors representing possible sources of variability: a linear trend term for long-term changes due to increases in GHGs and ozone depleting substances, and a set of proxy indices for ENSO, the 11 yr solar cycle, the QBO and volcanic eruptions.

Valuable information about the impact of each forcing can be extracted with this method, provided that the correct portion of variance in the predictand time series is fit, along with its relative attribution to each of the predictors. However, this is not the case when the predictors in matrix $\mathbf{X}$ are cross correlated ("multi-collinearity"), and when there is autocorrelation in the predictand time series ("persistence") (Wilks, 2011). Spurious correlations with the predictors can arise due to persistence in the predictand time series, while multi-collinearity leads to erroneous partitioning of the variance among predictors. Collinearity between the predictors can be significant, especially in relatively short records; an example is the correlation found between the N3.4 index and the 11 yr solar cycle (Marsh and Garcia, 2007). Additionally, significant persistence can be found within seasonal time scales in atmospheric field variables, which implies that individual data points in the predictand are not independent.

A common way to circumvent the problem associated with persistence is to treat the residual error term in the regression model as an autoregressive process (Tiao et al., 1990). This method implies correction of both the basis functions in $\mathbf{X}$ and the

ACPD
13, 30097–30142, 2013

predictand Y with the autocorrelation coefficient of the residual error term ϵ estimated from a first application of the regression model. This intermediate step is called "pre-whitening", and its application can be found in numerous papers on the solar signal in the stratosphere (e.g., Soukharev and Hood, 2006; Austin et al., 2008; Frame and Gray, 2010). Another way to account for autocorrelation is by pre-whitening the predictand Y and predictors $\mathbf{X}$ with the first order autocorrelation coefficient of the original time series of the predictand Y. This is the so-called Box-Jenkins (BJ) methodology (Box and Jenkins, 1980).

Both pre-whitening techniques were carried out on the output from the WACCM model. It was found that the BJ pre-whitening leads to an autocorrelation function (ACF) that is closer to white noise (not shown), and hence optimal for regression analysis (Box and Jenkins, 1980). Hence, the BJ technique was chosen for the analysis of the simulations presented in this paper.

Once the time series have been prewhitened, the regression model equation is carefully assessed upon analysis of the lagged cross correlation structures between the predictors (i.e., the i time series in the $\mathbf{X}$ matrix), and the predictand Y. This is done to identify the lags that maximize the projection of variance onto the basis functions, improving the fit accuracy.

We performed a preliminary analysis by using both (i) deseasonalized monthly mean, (ii) seasonal mean (3-months averages) and (iii) 3-months running mean anomalies of temperature and ozone. It is found that the use of (ii) seasonal averages filters spurious cross correlation structures showing up at high frequencies (1–2 months) that are related to internal noise rather than a causal relationship. Therefore, seasonal mean anomalies are used in this analysis. The use of seasonal averages is also justified physically. Part of the changes in stratospheric temperature and ozone due to ENSO, QBO and solar cycle are mediated by changes in upwelling rates, especially in the TLS. Randel et al. (2002) showed that coherence between temperature and upwelling rates in the TLS is enhanced at seasonal time scales compared to higher frequen-

ACPD
13, 30097–30142, 2013

cies, so that dynamically forced changes in temperature can be better captured with seasonal averages.

In the reference "all forcings" ensemble, the matrix **X** reads as follows

$$\mathbf{X} = \begin{pmatrix} t \\ N3.4 \\ \mathrm{UV} \\ u30 \\ u10 \\ \mathrm{SAD} \end{pmatrix} \tag{A2}$$

where t is the time dimension in seasons, $N3.4$ is the Niño 3.4 index (the standardized mean sea surface temperature between 5° S–5° N latitude and 120–170° W longitude) for ENSO; UV is the ultraviolet solar radiation flux integrated in the Hartley band (240–270 nm) from the Lean dataset (Lean et al., 2005), and is used as a proxy for the 11 yr solar cycle; $u30$ and $u10$ are the equatorial zonal mean zonal winds at 30 and 10 hPa, which have the quality of being nearly orthogonal proxies for the QBO (Randel and Wu, 1996). SAD is the global mean surface area density at 50 hPa (in units $\mathrm{cm}^2\,\mathrm{cm}^{-3}$) of sulphate aerosol taken from the SAGE II dataset. Based on SAD, an aerosol mass distribution is assumed in WACCM3.5 for heating rate calculations (Tilmes et al., 2009). Hence, this dataset is the most appropriate proxy for the volcanic forcing in the model simulations.

When using data from the idealized ensembles, the forcings which are kept constant (following table 1) are removed from the **X** matrix. The N3.4 index is excluded in the "fixedSSTs" ensemble, u_{10} and u_{30} are excluded in the "noQBO" ensemble, while the SAD index is excluded in the "noVOLC" ensemble.

ACPD
13, 30097–30142, 2013

The first step in the formulation of the regression model is pre-whitening of both sides of Eq. (A1):

$$Y'_{t,z} = Y_{t,z} - \rho_z Y_{t-1,z}$$
$$\mathbf{X}'_{t,i,z} = \mathbf{X}_{t,i,z} - \rho_z \mathbf{X}_{t-1,i,z} \quad \text{(A3)}$$

where ρ_z is the autocorrelation coefficient of Y at lag of 1 season and at the level z, i is the forcing index. Equation (A3) is applied at each discrete model level z ranging from 0.1 hPa to 100 hPa. It is found that the use of the autocorrelation at lag 1 is enough to reduce the ACF of Y' to white noise, so that there is no need to use autoregressive models of higher order.

After pre-whitening both forcings and seasonal mean anomalies of temperature and ozone, we calculate the lag τ at which the absolute value of the cross correlation between each predictor i and Y' reaches a maximum value at a given level z.

$$\tau_{i,z} = t \| r(Y'_{t=0\ldots n,z}, \mathbf{X}'_{i,t=0+\tau\ldots n,z}) = \text{MAX} \quad \text{(A4)}$$

A separate analysis showed that no significant cross correlation between predictors is introduced by using the 1 yr window. Furthermore, correlations arising at lags larger than the characteristic time scale of each forcing are unlikely to describe a physical link with the dependent variable. This is especially true in the stratosphere, where the responses are not modulated by the ocean. We also constrain both u_{30} and u_{10} indices to have the same value τ, since the use of different lags would introduce correlations between them, and thus loss of orthogonality.

An additional complication in this analysis is posed by the separation of QBO signals from other sources of variability. We found that the observed zonal wind which is assimilated in the ensembles including a QBO contains significant variations arising from volcanoes, ENSO and solar cycle. For the solar cycle, this result is consistent with the reported modulation of the QBO periodicity by the solar cycle (Salby and Callaghan,

ACPD
13, 30097–30142, 2013

2000). We remove the collinearity by computing two filtered QBO indices. For this purpose, we regress the solar cycle, ENSO and volcanoes on zonal mean wind at both 30 and 10 hPa, and take the residual as filtered QBO index, as described by the Eq. (A5).

$$u30^{*}_{t,z} = u30'_{t,z} - (\beta_{\mathrm{uv}} UV'_{t-\tau_{i=\mathrm{uv},z},z} + \beta_{\mathrm{enso}} N3.4'_{t-\tau_{i=\mathrm{enso},z},z} + \beta_{\mathrm{volc}} \mathrm{SAD}'_{t-\tau_{i=\mathrm{volc},z},z})$$
$$u10^{*}_{t,z} = u10'_{t,z} - (\beta_{\mathrm{uv}} UV'_{t-\tau_{i=\mathrm{uv},z},z} + \beta_{\mathrm{enso}} N3.4'_{t-\tau_{i=\mathrm{enso},z},z} + \beta_{\mathrm{volc}} \mathrm{SAD}'_{t-\tau_{i=\mathrm{volc},z},z}) \quad \text{(A5)}$$

In this way, the $u30^{*}$ and $u10^{*}$ are made orthogonal with respect to the other indices, thus improving the accuracy of the regression analysis. The two filtered QBO indices, along with the prewhitened and lagged predictors are then used in the target regression model for ozone and temperature.

$$Y'_{t,z} = \beta'_{\mathrm{uv}} UV'_{t-\tau_{i=\mathrm{uv},z},z} + \beta'_{\mathrm{enso}} N3.4'_{t-\tau_{i=\mathrm{enso},z},z} + \beta'_{\mathrm{qbo1}} u30^{*}_{t,z} + \beta'_{\mathrm{qbo2}} u10^{*}_{t,z} + \beta'_{\mathrm{volc}} \mathrm{SAD}'_{t-\tau_{i=\mathrm{volc},z},z} + e'_{t,z} \quad \text{(A6)}$$

The regression model described by Eq. (A6) is used in the analysis of the reference "all forcings" set. In the idealized sets, the forcings which are kept fixed are excluded from the Eq. (A6).

Acknowledgements. The authors thank J. Añel for performing one of the simulations. The authors thank High-performance computing support from Yellowstone (ark:/85065/d7wd3xhc) provided by NCAR's Computational and Information System Laboratory, sponsored by the National Science Foundation. Computing resources were also provided by the Barcelona Supercomputing Center (BSC), Centro Extremeño de iNvestigación, Innovación Tecnológica y Supercomputacion (CENITS), and Centro de Supercomputación de Galicia (CESGA). The author thankfully acknowledges the technical expertise and assistance provided by BSC, CENITS and CESGA for carrying out the model simulations in the MareNostrum, Lusitania and Finisterrae supercomputers. The author also acknowledges the European COST Action ES1005. G.

ACPD
13, 30097–30142, 2013

Chiodo was supported by the Spanish Ministry of Education in the framework of the “FPU” doctoral fellowship (grant AP2009-0064), and the Spanish Project CONSOLIDER (grant CSD2007-00050-II-PR4/07). The National Center for Atmospheric Research is operated by the University Corporation for Atmospheric Research under sponsorship of the National Science Foundation.

References

Austin, J., Tourpali, K., Rozanov, E., Akiyoshi, H., Bekki, S., Bodeker, G., Brühl, C. Butchart, N., Chipperfield, M., Deushi, M., Fomichev, V. I., Giorgetta, M. a., Gray, L., Kodera, K., Lott, F., Manzini, E., Marsh, D., Matthes, K., Nagashima, T., Shibata, K., Stolarski, R. S., Struthers, H., and W. Tian: Coupled chemistry climate model simulations of the solar cycle in ozone and temperature, J. Geophys. Res., 113, 1–20, 2008. 30099, 30122

Baldwin, M., Gray, L. J., Dunkerton, T. J., Hamilton, K., Haynes, P. H., Randel, W. J., Holton, J. R., Alexander, M. J., Hirota, I., Horinouchi, T., Jones, D.B.A., Kinnersley, J.S., Marquardt, C., Sato, K., and M. Takahashi: The quasi-biennial oscillation, Rev. Geophys., 39, 179–230, 2001. 30107

Bisgaard, S. and M. Kulahci: Time Series Analysis and Forecasting by Example, vol. 815, Wiley, Singapore, 2011. 30104

Box, G. and Jenkins, G.: Time Series Analysis, Forecasting and Control, Holder Day, San Francisco, 1980. 30104, 30122

Calvo, N., Garcia, R., Randel, W., and Marsh, D. R.: Dynamical mechanism for the increase in tropical upwelling in the lowermost tropical stratosphere during warm enso events, J. Atmos. Sci., 67, 2331–2340, 2010. 30107

CCMVal-2: SPARC CCMVal Report on the Evaluation of Chemistry–Climate Models, edited by: Eyring, V., Shepherd, T. G., and Waugh, D. W., Tech. rep., SPARC Report No. 5, WCRP-132, WMO/TD-No. 1526, World Meteorological Organization, Geneva, 2010. 30103

Chiodo, G., Calvo, N., Marsh, D. R., and Garcia-Herrera, R.: The 11 year solar cycle in transient WACCM3.5 simulations, J. Geophys. Res., 117, D06109, doi:10.1029/2011JD016393, 2012. 30099, 30102, 30103, 30116, 30119

Crooks, S. and Gray, L.: Characterization of the 11-year solar signal using a multiple regression analysis of the ERA-40 dataset, J. Climate, 18, doi:10.1175/JCLI-3308.1, 2005. 30099, 30105

ACPD
13, 30097–30142, 2013

Diaz, J., Garcia, R., De Castro, F. V., Hernández, E., López, C., and Otero, A.: Effects of extremely hot days on people older than 65 years in Seville (spain) from 1986 to 1997, Int. J. Biometeorol., 46, 3, 145–149, 2002a. 30104

Diaz, J., Jordán, A., García, R., López, C., Alberdi, J., Hernández, E., and Otero, A.: Heat waves in Madrid 1986–1997: effects on the health of the elderly, Int. Arch. Occ. Env. Hea., 75, 163–170, 2002b. 30104

Eyring, V., Cionni, I., Bodeker, G. E., Charlton-Perez, A. J., Kinnison, D. E., Scinocca, J. F., Waugh, D. W., Akiyoshi, H., Bekki, S., Chipperfield, M. P., Dameris, M., Dhomse, S., Frith, S. M., Garny, H., Gettelman, A., Kubin, A., Langematz, U., Mancini, E., Marchand, M., Nakamura, T., Oman, L. D., Pawson, S., Pitari, G., Plummer, D. A., Rozanov, E., Shepherd, T. G., Shibata, K., Tian, W., Braesicke, P., Hardiman, S. C., Lamarque, J. F., Morgenstern, O., Pyle, J. A., Smale, D., and Yamashita, Y.: Multi-model assessment of stratospheric ozone return dates and ozone recovery in CCMVal-2 models, Atmos. Chem. Phys., 10, 9451–9472, doi:10.5194/acp-10-9451-2010, 2010. 30103

Calvo-Fernández, N. C., Garcia-Herrera, R., Puyol, D. G., Hernandez, E., GarcÍa, R., Gimeno, L., and Ribera, P.: Analysis of the enso signal in tropospheric and stratospheric temperatures observed by msu, 1979–2000, J. Climate, 17, 3934–3946, 2004. 30100

Frame, T. and Gray, L.-J.: The 11-year solar cycle in era-40 data: an update to 2008, J. Climate, 23, 2213–2222, 2010. 30099, 30100, 30105, 30116, 30117, 30120, 30122

Garcia, R., Marsh, D. R., Kinnison, D., Boville, B., and Sassi, F.: Simulation of secular trends in the middle atmosphere, 1950–2003, J. Geophys. Res., 112, D09301, doi:10.1029/2006JD007485, 2007. 30101, 30103, 30119

Gray, L., Beer, J., Geller, M., Haigh, J. D., Lockwood, M., Matthes, K., Cubasch, U., Fleitmann, D., Harrison, G., Hood, L., Luterbacher, J., Meehl, G. A., Shindell, D., Van Geel, B., and White, W.: Solar influences on climate, Rev. Geophys., 48, RG4001, 1–53, 2010. 30099, 30107

Haigh, J. and Blackburn, M.: Solar influences on dynamical coupling between the stratosphere and troposphere, Space Sci. Rev., 125, 331–344, 2006. 30101

Hood, L.: The solar cycle variation of total ozone: dynamical forcing in the lower stratosphere, J. Geophys. Res., 102, 1355–1370, 1997. 30099

Hood, L. and Soukharev, B.: Quasi-decadal variability of the tropical lower stratosphere: the role of extratropical wave forcing, J. Atmos. Sci., 60, 2389–2403, 2003. 30099

ACPD
13, 30097–30142, 2013

Hood, L., Soukharev, B., and McCormack, J.: Decadal variability of the tropical stratosphere: secondary influence of the el niño–southern oscillation, J. Geophys. Res., 115, D11113, doi:10.1029/2009JD012291, 2010. 30100, 30108

Hurrell, J. W., Hack, J. J., Shea, D., Caron, J. M., and Rosinski, J.: A new sea surface temperature and sea ice boundary dataset for the community atmosphere model, J. Climate, 21, 5145–5153, 2008. 30103, 30131

Kodera, K. and Kuroda, Y.: Dynamical response to the solar cycle, J. Geophys. Res., 107, 4749, doi:10.1029/2002JD002224, 2002. 30099

Lean, J., Rottman, G., Harder, J., and Kopp, G.: Sorce contributions to new understanding of global change and solar variability, The Solar Radiation and Climate Experiment (SORCE), Sol. Phys., 230, 27–53, 2005. 30103, 30123, 30131

Lee, H. and Smith, A.: Simulation of the combined effects of solar cycle, quasi-biennial oscillation, and volcanic forcing on stratospheric ozone changes in recent decades, J. Geophys. Res., 108, D24049, doi:10.1029/2001JD001503, 2003. 30101, 30118

Marsh, D. R. and Garcia, R.: Attribution of decadal variability in lower-stratospheric tropical ozone, Geophys. Res. Lett., 34, L21807, doi:10.1029/2007GL030935, 2007. 30101, 30107, 30108, 30118, 30119, 30121

Matthes, K., Marsh, D., Garcia, R., Kinnison, D., Sassi, F., and Walters, S.: Role of the QBO in modulating the influence of the 11 year solar cycle on the atmosphere using constant forcings, J. Geophys. Res., 115, D18110, doi:10.1029/2009JD013020, 2010. 30103, 30131

Meehl, G., Arblaster, J., Matthes, K., Sassi, F., and van Loon, H.: Amplifying the Pacific climate system response to a small 11-year solar cycle forcing, Sci., 325, 5944, 1114–1118, 2009. 30107

Pap, J. and Fox, P.: Solar variability and its effects on climate, American Geophysical Union Geophysical Monograph Series, Washington DC, 141, 2003. 30107

Randel, W. and Wu, F.: Isolation of the ozone QBO in SAGE 2 data by singular-value decomposition, J. Atmos. Sci., 53, 2546–2560, 1996. 30105, 30123

Randel, W. and Wu, F.: A stratospheric ozone profile data set for 1979–2005: variability, trends, and comparisons with column ozone data, J. Geophys. Res, 112, D06313, doi:10.1029/2006JD007339, 2007. 30100, 30117, 30118

Randel, W., Garcia, R., Calvo, N., and Marsh, D.: ENSO influence on zonal mean temperature and ozone in the tropical lower stratosphere, Geophys. Res. Lett, 36, L15822, doi:10.1029/2009GL039343, 2009. 30100

ACPD
13, 30097–30142, 2013

Randel, W. J., Wu, F., Russell, J., Waters, J., and Froidevaux, L.: Ozone and temperature changes in the stratosphere following the eruption of mount pinatubo, J. Geophys. Res., 100, 16753–16764, 1995. 30100

Randel, W. J., Garcia, R. R., and Wu, F.: Time-dependent upwelling in the tropical lower stratosphere estimated from the zonal-mean momentum budget, J. Atmos. Sci., 59, 2141–2152, 2002. 30122

Randel, W. J., Shine, K. P., Austin, J., Barnett, J., Claud, C., Gillett, N. P., Keckhut, P., Langematz, U., Lin, R., Long, C., Mears, C., Miller, A., Nash, J., Seidel, D.J., Thompson, D.W.J., Wu, F., and S. Yoden: An update of observed stratospheric temperature trends, J. Geophys. Res., 114, D02107, doi:10.1029/2008JD010421, 2009. 30100, 30105

Rienecker, M. M., Michele, M., Suarez, M. J., Gelaro, R., Todling, R., Bacmeister, J., Liu, E., Bosilovich, M. G., Schubert, S. D, Takacs, L., Kim, G.-K., Bloom,S., Chen,J., Collins,D., Austin, C., da Silva, A., Wei Gu, Joiner, J., Koster, R.D., Lucchesi,R., Molod,A., Owens,T., Pawson, S., Pegion, P., Redder, C.R., Reichle, R., Robertson, F.R., Ruddick, A.G., Sienkiewicz, M., and J.Woollen: Merra: Nasa's modern-era retrospective analysis for research and applications, J. Climate, 24, 3624–3648, 2011. 30113

Robock, A.: Volcanic eruptions and climate, Rev. Geophys., 38, 191–219, 2000. 30107, 30108

Salby, M. and Callaghan, P.: Connection between the solar cycle and the qbo: the missing link*, J. Climate, 13, 2652–2662, 2000. 30124

Schmidt, H., Brasseur, G., and Giorgetta, M.: Solar cycle signal in a general circulation and chemistry model with internally generated quasi biennial oscillation, J. Geophys. Res., 115, D00I14, doi:10.1029/2009JD012542, 2010. 30099

Smith, A. and Matthes, K.: Decadal-scale periodicities in the stratosphere associated with the solar cycle and the QBO, J. Geophys. Res., 113, D05311, doi:10.1029/2007JD009051, 2008. 30101, 30118

Soukharev, B. and Hood, L.: Solar cycle variation of stratospheric ozone: multiple regression analysis of long-term satellite data sets and comparisons with models, J. Geophys. Res., 111, D20314, doi:10.1029/2006JD007107, 2006. 30099, 30100, 30117, 30118, 30120, 30122

Thomason, L., Poole, L., and Deshler, T.: A global climatology of stratospheric aerosol surface area density deduced from stratospheric aerosol and gas experiment ii measurements: 1984–1994, J. Geophys. Res., 102, 8967–8976, 1997. 30103, 30131

ACPD
13, 30097–30142, 2013

Tiao, G., Reinsel, G., Xu, D., Pedrick, J., Zhu, X., Miller, A., DeLuisi, J., Mateer, C., and Wuebbles, D.: Effects of autocorrelation and temporal sampling schemes on estimates of trend and spatial correlation, J. Geophys. Res., 95, 20507–20517, 1990. 30100, 30121

Tilmes, S., Garcia, R., Kinnison, D., Gettelman, A., and Rasch, P.: Impact of geoengineered aerosols on the troposphere and stratosphere, J. Geophys. Res., 114, D12305, doi:10.1029/2008JD011420, 2009. 30103, 30123

Wilks, D. S.: Statistical Methods in the Atmospheric Sciences, vol. 100, Academic press, The Netherlands, 2011. 30121

ACPD
13, 30097–30142, 2013

Table 1. Table of the performed WACCM3.5 ensembles.

name	SSTs	QBO	volcanoes	solar
"all forcings" (2)	observed (Hurrell et al., 2008)	assimilated (Matthes et al., 2010)	SAGE II (Thomason et al., 1997)	(Lean et al., 2005)
"fixedSSTs"(2)	climatological	assimilated (Matthes et al., 2010)	SAGE II (Thomason et al., 1997)	(Lean et al., 2005)
"noQBO" (2)	observed (Hurrell et al., 2008)	none (weak east)	SAGE II (Thomason et al., 1997)	(Lean et al., 2005)
"noVOLC" (2)	observed (Hurrell et al., 2008)	assimilated (Matthes et al., 2010)	climatological	(Lean et al., 2005)

ACPD
13, 30097–30142, 2013

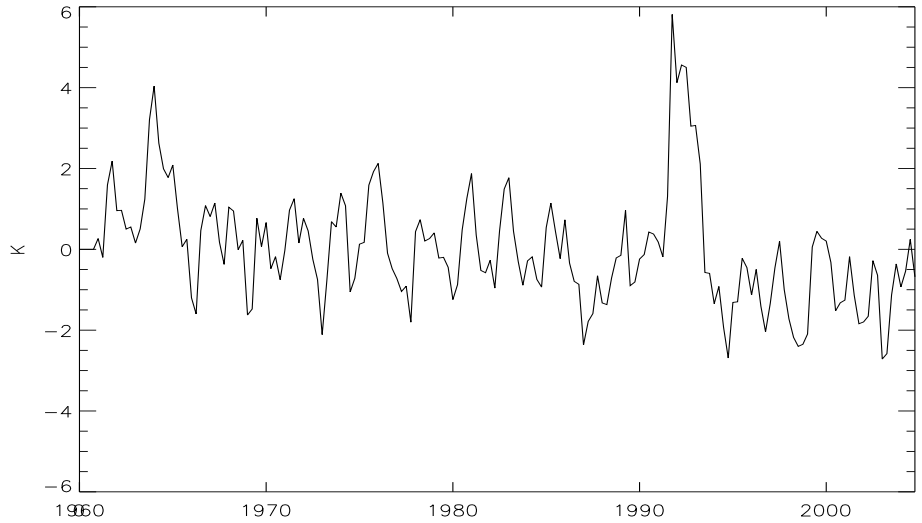

Fig. 1. Time-series of the simulated seasonal mean temperature anomalies at 50 hPa, averaged over the tropics (25° N–25° S) in the reference "all forcings" set. Units K.

ACPD
13, 30097–30142, 2013

The solar signal in the tropical stratosphere

G. Chiodo et al.

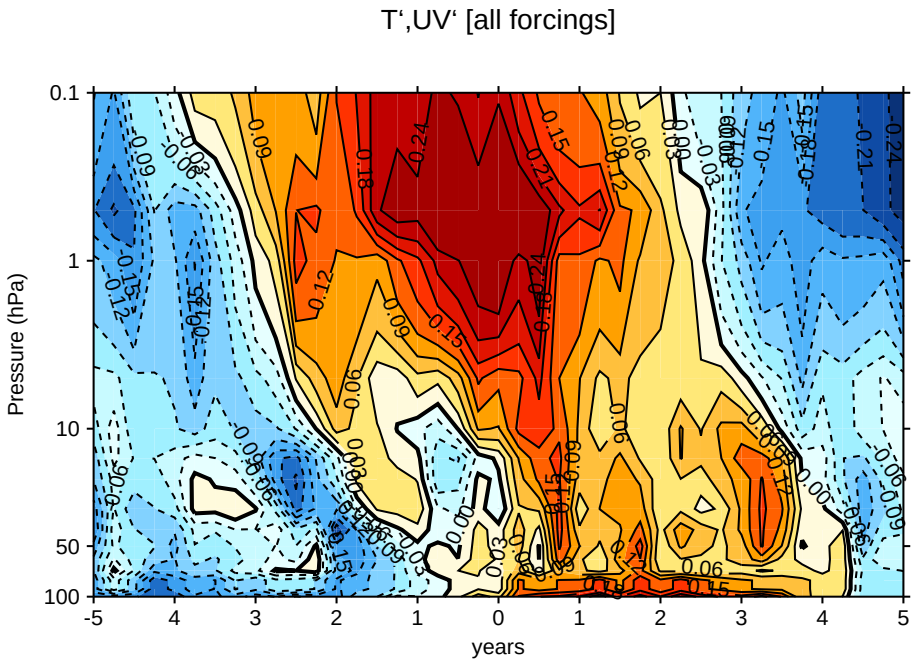

Fig. 2. Lag correlation between the tropical mean (25° N–25° S) prewhitened seasonal mean temperature from the "all forcings" case and the UV radiation index. Positive lags mean that UV predictor leads temperature changes. Solid contours and red colors denote positive correlations, while dashed contours and blue colors indicate negative correlations. Contours are drawn every 0.03.

ACPD
13, 30097–30142, 2013

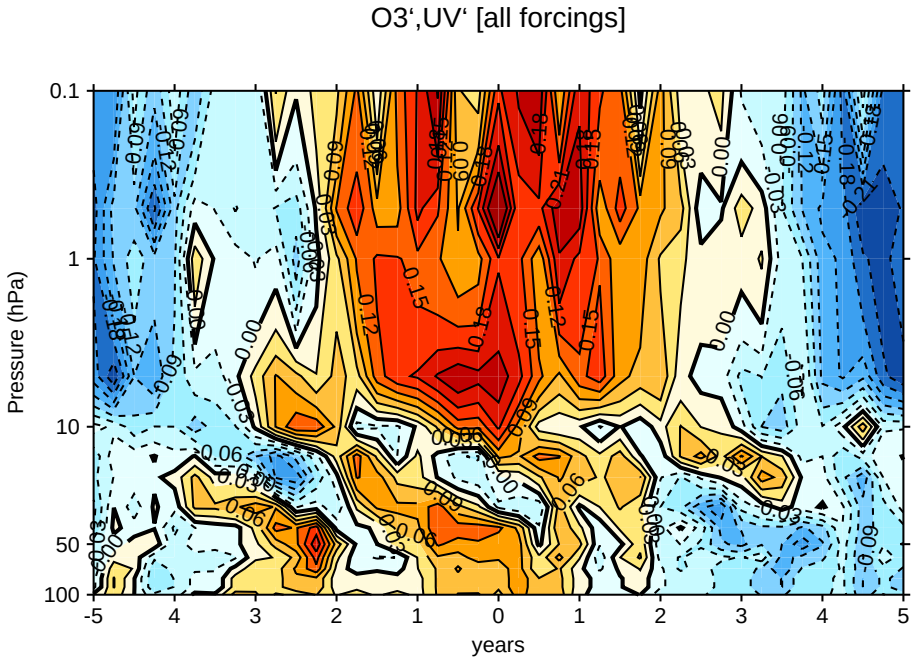

Fig. 3. As in Fig. 2, for tropical mean zonal mean ozone from the "all forcings" case.

ACPD
13, 30097–30142, 2013

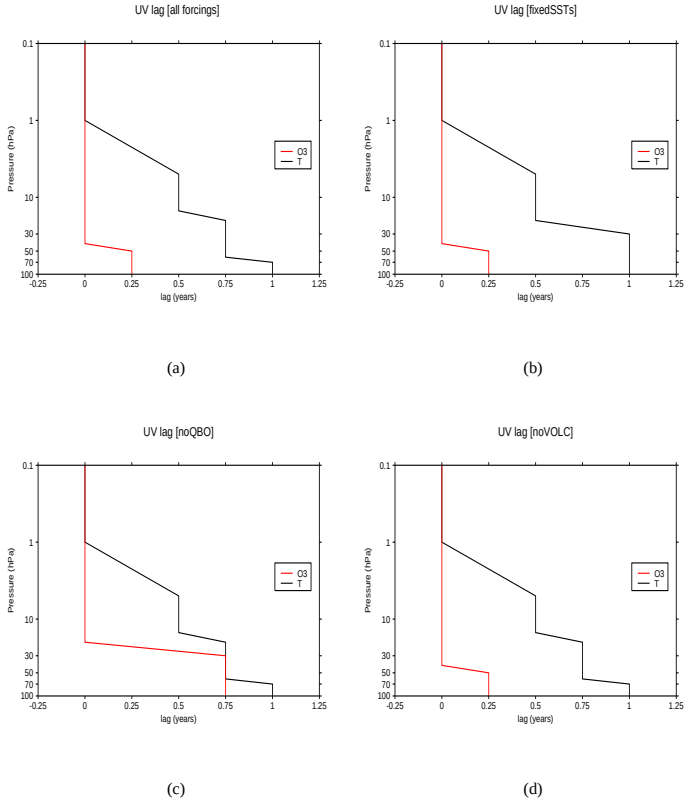

Fig. 4. Vertical profile of the lag that maximises the absolute value of the correlation (in the 0–1 yr window) between UV radiation and prewhitened seasonal mean temperature (black) and ozone (red); from **(a)** the "all forcings", **(b)** "fixedSSTs", **(c)** "noQBO", and **(d)** "noVOLC" sets. The values are introduced as $\tau_{i=\mathrm{UV}}$ in Eq. (A6) for regression of tropical mean temperature and ozone.

ACPD
13, 30097–30142, 2013

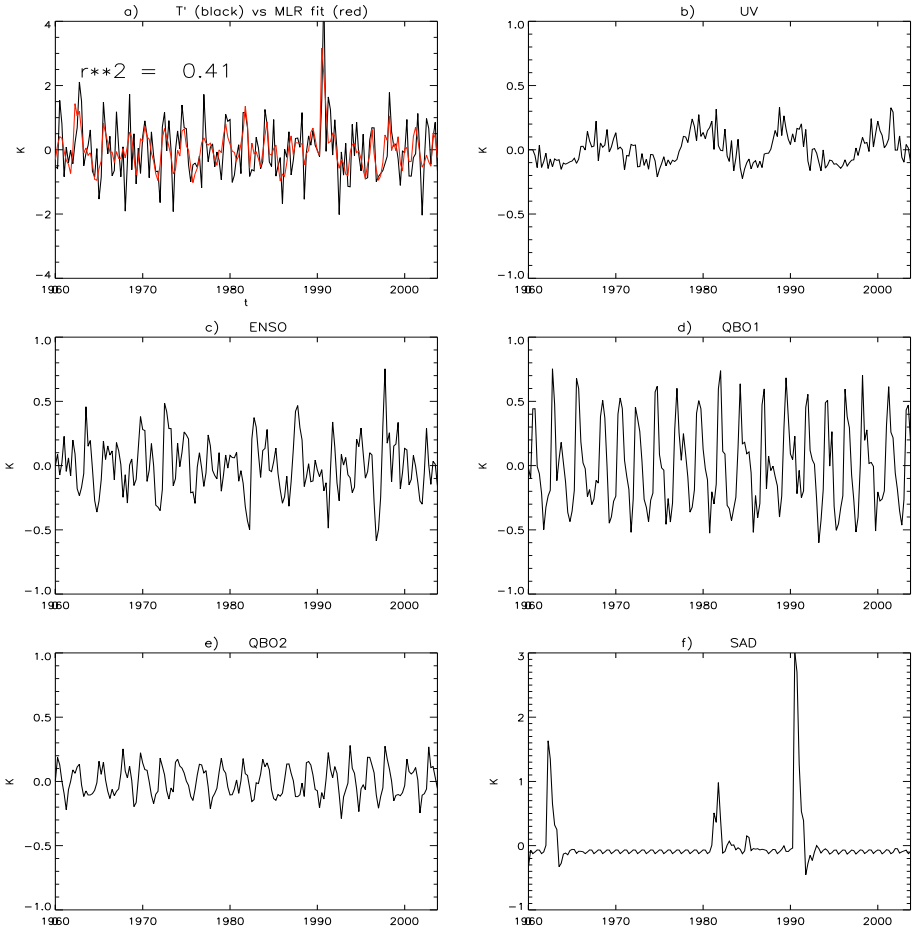

Fig. 5. (a) Time-series of tropical average seasonal mean zonal mean temperature anomalies at 50 hPa after pre-whitening (black), along with the regression fit from Eq. (A6) (red); **(b–f)** Contribution of each of the terms on the right hand side of Eq. (A6) to the regression fit.

ACPD
13, 30097–30142, 2013

The solar signal in the tropical stratosphere

G. Chiodo et al.

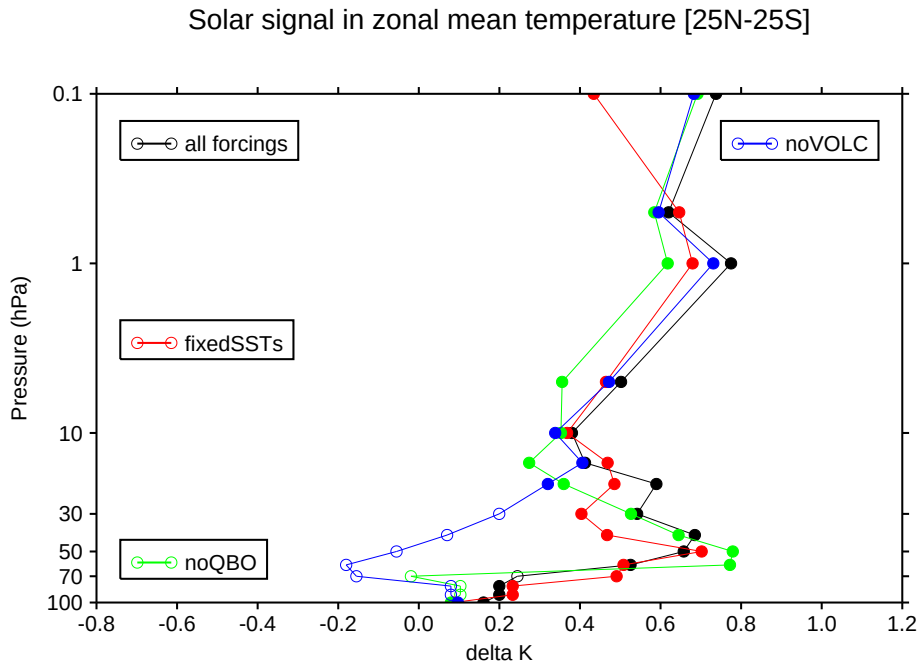

Fig. 6. Solar signal in zonal mean temperature, estimated as the UV regression coefficient (β'_{UV} in Eq. A6) multiplied by 0.175, which represents the 2σ variation of the UV index used in the MLR. Delta K units denote the relative solar cycle peak to trough change in Kelvin. Filled dots indicate that the derived regression coefficients are significantly different from 0 at the 2σ significance level. The lags used for the UV index in each experiment set is the black line shown in Fig. 4.

ACPD
13, 30097–30142, 2013

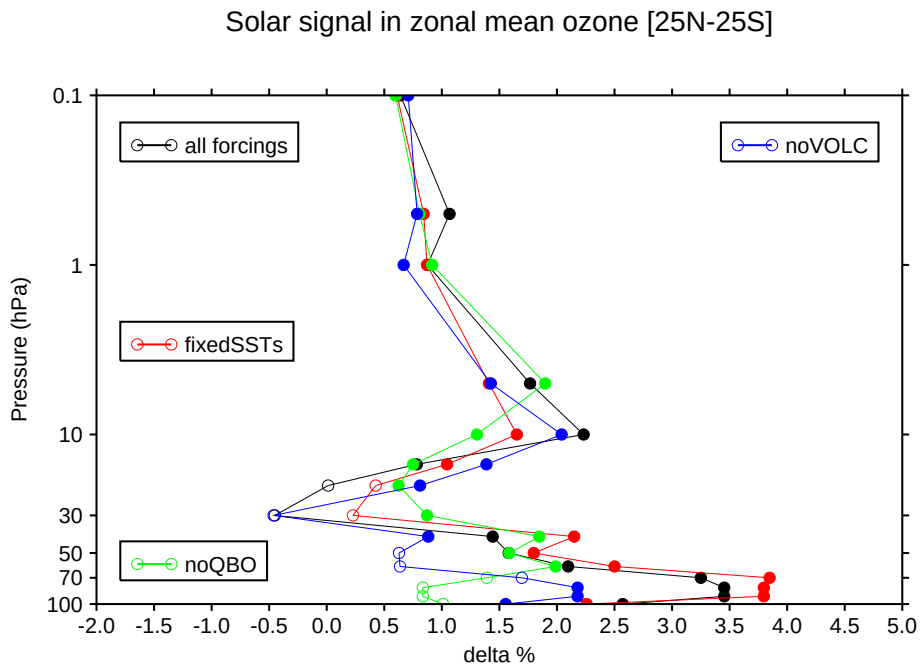

Fig. 7. As in Fig. 7, for tropical mean zonal mean ozone. Delta % units denote the relative solar cycle peak to trough change in %. Filled dots indicate that the derived regression coefficients are significantly different from 0 at the 2σ significance level. The lags used for the UV index in each experiment set is the red line shown in Fig. 4.

ACPD
13, 30097–30142, 2013

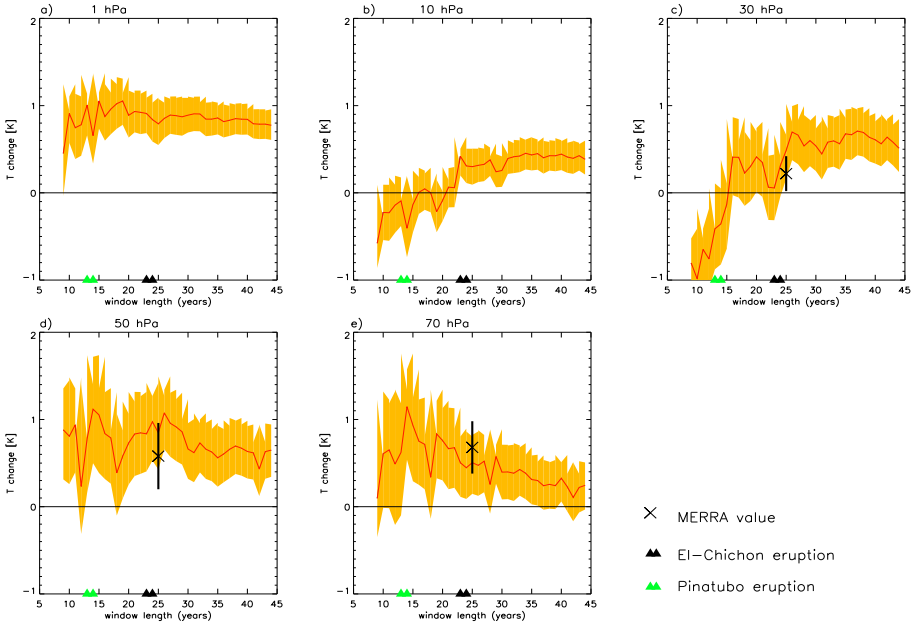

Fig. 8. UV regression coefficient (β'_{UV} in Eq. A6) in tropical mean zonal mean temperature (red line) along with the 2σ uncertainty (yellow shading) from the "all forcings" case, plotted as a function of the window used (in years). The endpoint of the window is the last available year in the ensembles, i.e., 2004. Results are shown for **(a)** 1 hPa, **(b)** 10 hPa, **(c)** 30 hPa, **(d)** 50 hPa, and **(e)** 70 hPa. Crosses show the values obtained from MERRA reanalysis at 30, 50 and 70 hPa using the window overlapping the simulation period (1979–2004). Units K.

ACPD
13, 30097–30142, 2013

The solar signal in the tropical stratosphere

G. Chiodo et al.

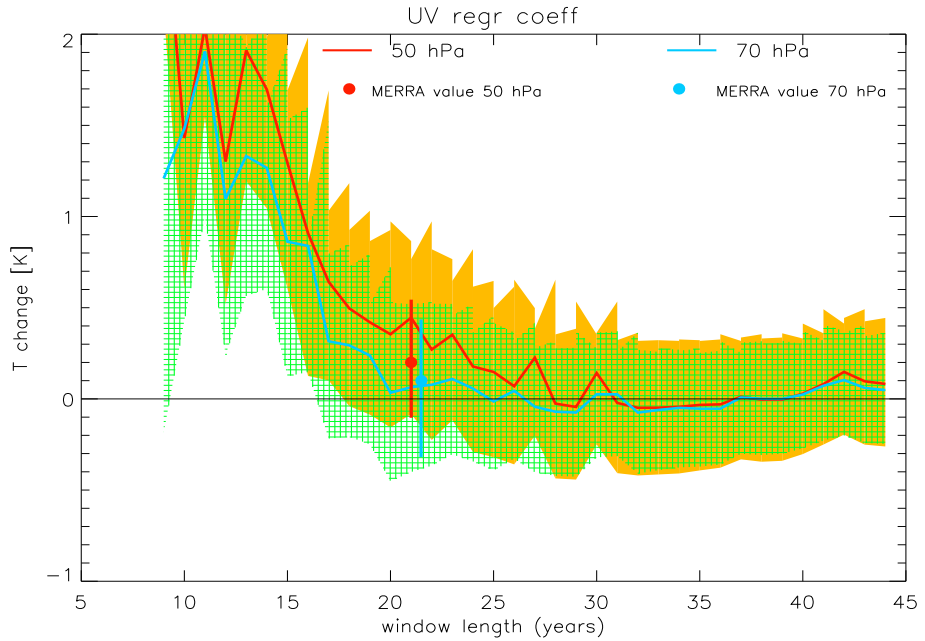

Fig. 9. UV regression coefficient in tropical mean zonal mean temperature from the "all forcings" case, obtained when omitting post El Chichón and Mt. Pinatubo data (see exact dates indicated in the text), plotted as a function of the years included in the window. The endpoint of the window is the last available year in the ensembles, i.e., 2004. Results are shown for the 50 hPa (red) and 70 hPa (blue) levels, along with the 2σ uncertainty (yellow for 50 hPa, and green for 70 hPa). Dots indicate the values obtained from MERRA reanalysis, along with the 2σ uncertainty. Units K.

ACPD
13, 30097–30142, 2013

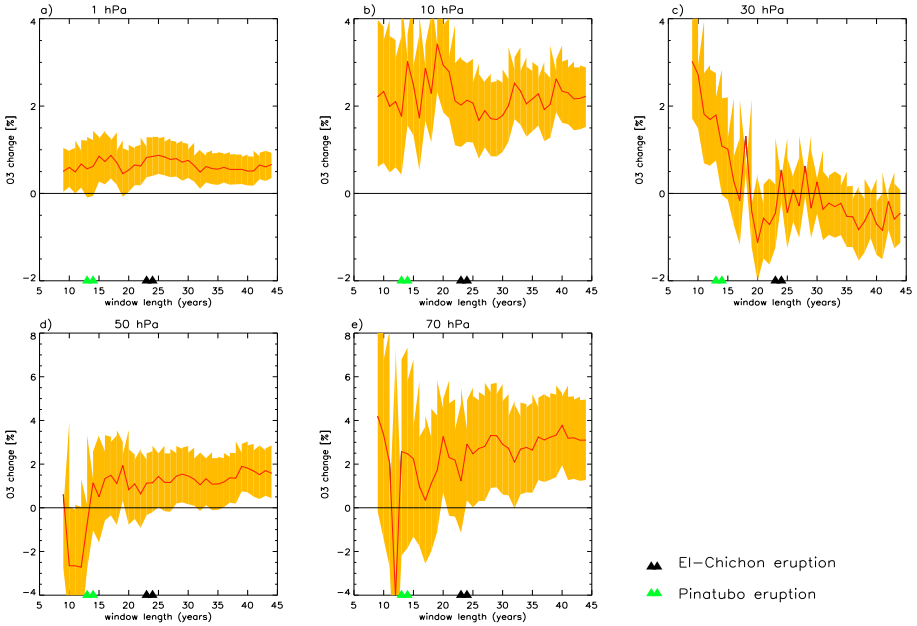

Fig. 10. As in Fig. 8, for tropical mean zonal mean ozone. Units % (i.e., relative change in concentration).

ACPD
13, 30097–30142, 2013

Fig. 11. UV regression coefficient in zonal mean ozone from the "all forcings" case, omitting the post El Chichón and Mt. Pinatubo data (June 1982 to November 1983, and September 1991 to November 1993), plotted as a function of the window used (in years) for 50 hPa (red) and 70 hPa (blue), along with the 2σ uncertainty (yellow shading for 50 hPa, and green shading for 70 hPa). The endpoint of the window is the last available year in the ensembles, i.e., 2004. Units %.

ACPD
13, 30097–30142, 2013